We are IntechOpen,
the world's leading publisher of Open Access books
Built by scientists, for scientists

4,800
Open access books available

122,000
International authors and editors

135M
Downloads

154
Countries delivered to

Our authors are among the

TOP 1%
most cited scientists

12.2%
Contributors from top 500 universities

CLARIVATE ANALYTICS
BOOK CITATION INDEX
INDEXED

WEB OF SCIENCE™

Selection of our books indexed in the Book Citation Index
in Web of Science™ Core Collection (BKCI)

Interested in publishing with us?
Contact book.department@intechopen.com

Numbers displayed above are based on latest data collected.
For more information visit www.intechopen.com

The Increase of the Micoporosity and CO$_2$ Adsorption Capacity of the Commercial Activated Carbon CWZ-22 by KOH Treatment

Joanna Sreńscek-Nazzal, Urszula Narkiewicz,
Antoni W. Morawski, Rafał J. Wróbel and
Beata Michalkiewicz

Additional information is available at the end of the chapter

Abstract

The chemical modification of CWZ-22—commercial activated carbon (AC) with KOH-to enhance CO$_2$ adsorption was examined. The effect of different impregnation ratios KOH:CWZ-22 from 1 to 4 was studied. The ACs were characterized by CO$_2$ and N$_2$ sorption, Fourier transform infrared (FTIR), SEM, and XRD methods.

The impregnation of CWZ-22 with KOH highly effectively increased the porosity, specific surface area, and pore volume of ACs. The specific surface area of KOH:CWZ-22 = 4 increased to 1299 m^2/g as compared with pristine, which is equal to 856 m^2/g. The total pore volume raised from 0.51 to 0.77 cm^3/g.

The chemical modification of CWZ-22 increased the CO$_2$ adsorption capacity up to 38%. The Sips model described very good CO$_2$ adsorption on KOH:CWZ-22 = 4 and pristine sample. The surface of both ACs was homogenous. The values of isosteric heats of adsorption indicated on physisorption.

Keywords: carbon dioxide, activated carbon, CWZ-22, KOH, CO$_2$ adsorption

1. Introduction

The emission of CO$_2$ originating mainly from industry has become a worldwide problem responsible for the global warming. The combustion of fossil fuel in power plants remains the

main point source for CO_2 emission to the atmosphere. Reduction in the CO_2 concentration in the atmosphere is currently a hot topic [1, 2]. Among technologies proposed for reduction in CO_2 emissions, adsorption is considered as a very promising process for CO_2 capture. Alternatively, solid-based adsorbents have drawn substantial attention for CO_2 capture.

Nowadays, many types of porous materials have been used in CO_2 adsorption, such as zeolites [3], metal–organic frameworks (MOFs) [4], porous silica [5], and activated carbons (ACs) [2, 6–9]. Among these adsorbents, activated carbon (AC) has drawn great attention recently because of its high adsorption capacity, low cost, availability, large surface area, an easy-to-design pore structure, hydrophobicity (insensitiveness to moisture), and low energy requirements for regeneration [10, 11]. The adsorption performance of activated carbons depends on the selection of carbon sources and activation conditions. It has been reported that the activated carbons prepared with commercial carpet [12], eucalyptus sawdust [13], yeast [14], palm shells [10], peanut shell [8], pitch [9], and molasses [15] had high adsorption capacity for CO_2.

Activated carbon can be mainly prepared by physical and chemical activation methods or by combination of both types of methods. Usually, physical activation is carried out using carbon dioxide, steam, air, or their mixture. Chemical activation involves agents such as zinc chloride [16], acids [17], and bases [10, 17]. KOH is one of the most widely used chemicals for activating the carbonaceous materials in preparation of activated carbon [1, 2, 8, 10]. Activated carbons obtained by chemical activation often possess a high specific surface area and well-developed micropores, which make them attractive materials for CO_2 adsorption. Particularly, KOH activation has been applied in the preparation of activated carbons because it can produce lots of micropores favorable for CO_2 adsorption. Therefore, the textural properties of the activated carbons depend on a type of carbon sources and the required amount of KOH for the preparation of efficient activated carbon to adsorb CO_2.

Our motivation was to increase the porosity and CO_2 adsorption capacity of commercial activated carbon CWZ-22. The increase of the CO_2 adsorption on commercial activated carbon modified using KOH has not been yet described.

2. Experimental method

2.1. Materials and sample preparation

A commercial activated carbon CWZ-22 (Gryfskand Sp. z o.o. Hajnówka, Poland) was used as the raw material in this work. The CWZ-22 samples were mixed with the saturated KOH solution. The mass ratio of KOH:CWZ-22 was varied from 1 to 4. The soaking time was 3 h. The mixtures were dried at 200°C. The impregnated sample was activated at temperature of 800°C for 1 h under nitrogen flow. Then, the samples were washed repeatedly with a 5 M solution of HCl and with distilled water until they were free of chlorine ions. Finally, these samples were dried at 200°C for 12 h. The materials were named as KOH:CWZ-22 = X, where X is the mass ratio of KOH:CWZ-22.

2.2. Characterization and adsorption analyses

The textural properties of the ACs were determined by physical adsorption of N_2 at 77 K and CO_2 at 273 K using a Quadrasorb apparatus (Quantachrome Instruments). Before the experiments, the samples were outgassed under vacuum at 250°C overnight. The specific surface area was measured by the multipoint BET (Brunauer–Emmet–Teller) method. The total pore volume, V_p, which includes both the micropores and the mesopores, was estimated from the amount of nitrogen adsorbed at the highest relative pressure. The micropore volume with diameter in the range of 0.31–1.47 nm was calculated by applying the NLDFT model for CO_2 adsorption at 273 K. Based on N_2 adsorption isotherm, the volume of micropores larger than 1.5 nm was obtained by applying the QSDFT method for the slit/cylinder pore model using the software provided by Quantachrome.

ACs were also analyzed by Fourier transform infrared (FTIR) on a Nicollet 380 (Thermo Scientific) spectrometer in order to identify the functional groups on the surface of the ACs. The CWZ-22 carbons were mixed with KBr. FTIR spectra were recorded within a range of 400–4000 cm^{-1}. The equipment was run prior to each actual measurement to record a background spectrum, which was then automatically subtracted from the spectrum of each analyzed sample.

The crystal structures of the samples were determined by XRD with the PANalytical Empyrean X-ray diffractometer using a Cu Kα radiation (α = 1.5418A°) at room temperature.

The surface morphology of the materials was performed by ultra-high resolution field emission scanning electron microscope (UHR FE-SEM Hitachi SU8020) equipped with the secondary electron (SE) detectors.

CO_2 adsorption isotherms were measured up to 2 bar at 25, 40, 60, 80, and 100°C temperature using the volumetric Sieverts' apparatus (IMI—Hiden Isochema Corporation). The CO_2 adsorption data were fitted to standard isotherm models such as Langmuir, Freundlich, Sips, and Toth.

The Langmuir Eq. (1) is based on the assumption of a structurally homogeneous adsorbent and is described by the following [6, 18, 19]:

$$q = \frac{q_m b_L p}{1 + (b_L p)} \tag{1}$$

where q is the adsorbed quantity (mmol of CO_2 per g of AC), p is the pressure of CO_2 in the bulk gas phase, q_m is the maximum adsorption capacity (mmol g^{-1}), and b_L is the Langmuir adsorption affinity constant (bar^{-1}).

The Freundlich isotherm is an empirical equation used to describe heterogeneous systems. The Freundlich Eq. (2) is expressed as [6, 19]:

$$q = k_F p^{n_F} \tag{2}$$

where k_F is the Freundlich constant, and n_F is the Freundlich heterogeneity factor. Value of $n_F > 1$ represents favorable adsorption. The higher n_F value implies higher sorption capacity, such as forming new adsorption sites.

The Sips adsorption isotherm model is a combined form of Langmuir and Freundlich models. The Sips adsorption equation is commonly given by the following nonlinear Eq. (3) [18, 20, 21]:

$$q = \frac{q_m b_s p^{n_s}}{1 + b_s p^{n_s}} \tag{3}$$

where b_s is the Sips adsorption affinity constant, and n_s is the Sips heterogeneity factor.

The Toth isotherm is a model useful in describing heterogeneous adsorption systems, which satisfies both low- and high-end boundaries of the concentration. The Toth's isotherm is expressed as Eq. (4) [20, 22, 23]:

$$q = \frac{q_m b_T p}{[1 + (b_T p)^{n_T}]^{1/n_T}} \tag{4}$$

where b_T is Toth adsorption affinity constant, and n_T is the Toth heterogeneity factor.

Isotherm parameters were obtained through a nonlinear fit of experimental data to the model equations using a MatCad software. In order to evaluate the fit of an isotherm to experimental equilibrium data, algorithms based on the Levenberg–Marquardt were used.

In this study, five nonlinear error functions were examined. In each case, a set of isotherm parameters were determined by minimizing the respective error function across the pressure range studied. The error functions employed were as follows: the correlation coefficient (R^2) [24], the sum of the squares of errors (SSE) [25], the hybrid fractional error function (HYBRID) [25], Marquardt's percent standard deviation (MPSD) [26], and the average relative error (ARE) [25].

Isosteric heats of adsorption (Q_i) can be calculated using Clausius–Clapeyron Eq. (5):

$$\left(\frac{\partial \ln(p)}{\partial \frac{1}{T}} \right)_\theta = \frac{Q_i}{R} \tag{5}$$

where ln(p) is the natural logarithm of the pressure at specific surface loading (θ), Q$_i$ is the isoteric heat of adsorption, R is the universal gas constant (8.314·10^{-3} kJ/mol·K), and T is the temperature [K]

The value of isosteric heats of adsorption was determined from the slop of ln(p) versus 1/T.

3. Results and discussion

3.1. Micropore size distribution of activated carbons

Figure 1 shows adsorption–desorption isotherms of N$_2$ at 77 K for the CWZ-22 and CWZ-22 modified by different amounts of KOH.
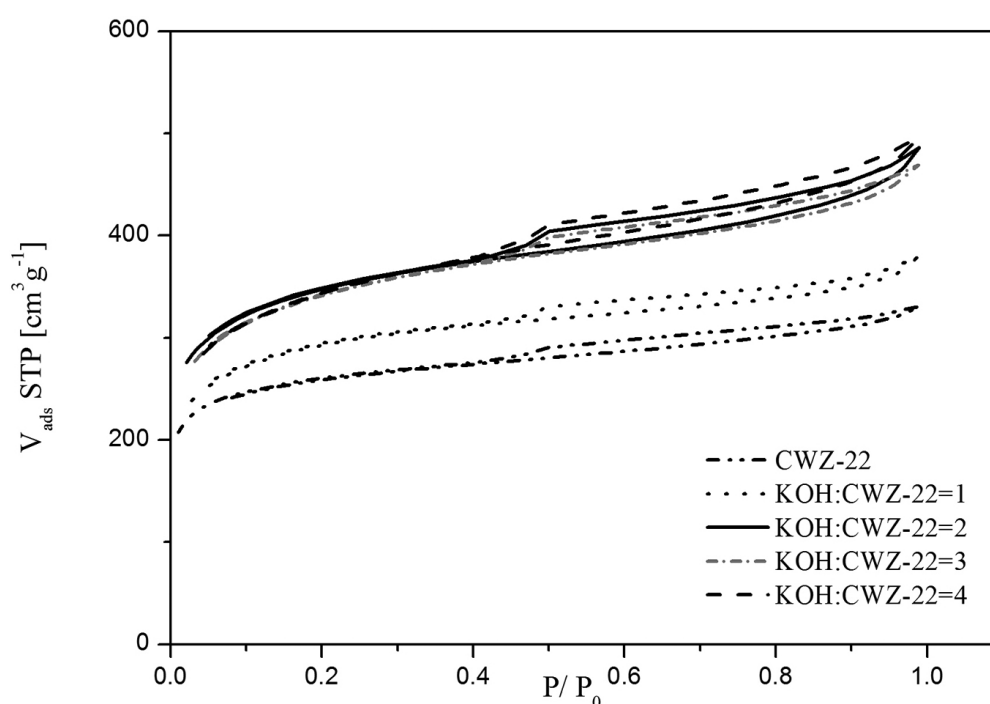

Figure 1. N$_2$ adsorption–desorption isotherms at 77 K for ACs.

All the isotherms present a high adsorption at low relative pressure, characteristic for micro-porous materials. The samples from KOH:CWZ-22 = 2–4 ratio showed the higher nitrogen adsorption capacity, whereas for the KOH:CWZ-22 = 1 and CWZ-22, nitrogen adsorption capacity was considerably lower. In addition, all samples showed hysteresis loop at relative pressure >0.4 indicating the presence of certain mesoporosity in the samples. The hysteresis loop type H4 was recognized, which is characteristic of slit shaped pores, such as those present in typical activated carbons. Thus, the isotherms of all samples appear to become a combination of types I and IV according to IUPAC classification. For the isotherms of AC with the highest impregnation ratio, the shape moves toward a type IV isotherm. This can be attributed to a formation of a greater fraction of mesoporosity, which is proved by the mesopore volume (**Table 1**). **Table 1** shows the textural properties of the activated carbons prepared with

different KOH:CWZ-22 ratios. Both specific surface area and total pore volume of the samples increased with increasing KOH:CWZ-22 ratios. When the KOH:CWZ-22 ratios are increased from 1 to 2 the specific surface area, total pore volume increases from 1093 to 1292 m^2 g^{-1} and from 0.59 to 0.75 cm^3 g^{-1}, respectively. However, further increase of KOH:CWZ-22 ratios only results in slow increase in specific surface area and pore volume. A similar situation can be observed in the case of micropores development. This may be due to the effect of the increase in small pores and the decomposition of porous structure.

AC	S_{BET} [m^2/g]	V_p [cm^3/g]	V_{mic} (N_2) 1.2–2 nm [cm^3/g]	V_{mic} (CO_2) 0.3–1.5 nm [cm^3/g]	V_{mes} [cm^3/g]
CWZ-22	856	0.51	0.34	0.24	0.17
KOH:CWZ-22 = 1	1093	0.59	0.34	0.31	0.25
KOH:CWZ-22 = 2	1292	0.75	0.38	0.32	0.37
KOH:CWZ-22 = 3	1256	0.73	0.38	0.32	0.35
KOH:CWZ-22 = 4	1299	0.77	0.40	0.37	0.37

Table 1. Textural data obtained by nitrogen (77 K) and CO_2 (273 K) isotherms, using BET and DFT methods.
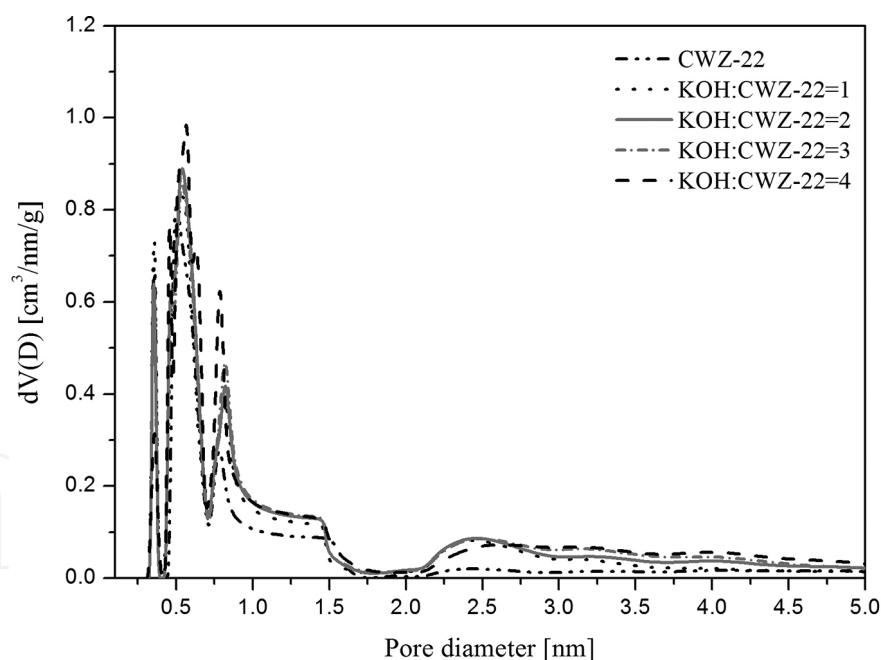

Figure 2. Pore size distribution of the CWZ-22 activated carbons prepared at different KOH:CWZ-22 mass ratio.

CO_2 and N_2 adsorption isotherms are commonly used to determine the pore size distribution of activated carbons. The pore size distribution is shown in **Figure 2**. All activated carbons have peaks in almost the same pore size ranges. One peak is located in the range of 0.3–0.4 nm, the second one in the range of 0.45–0.7 nm, the next in the range of 0.7–0.9 nm, and then in the range of 2.1–4.0 nm. The micropores are dominant. The volume of mesopores (pores

above 2 nm) is low. The pores with a diameter of more than 5 nm were no found. The pore volume of KOH:CWZ-22 = 4 at the pore size of above 0.45–0.7 nm and in the range of 0.7–0.9 nm is larger than for other carbons, indicated on a better developed microporous structure.

3.2. Surface morphology of activated carbon

The SEM images of the pristine CWZ-22 and modified CWZ-22 are shown in **Figure 3**. The surface of CWZ-22 was relatively smooth without large cavities except for some occasional cracks or crevices. All modified CWZ-22 samples have external surfaces covered with irregular holes of different sizes and the irregular shapes. It can be seen from the SEM images that the external surface of the activated carbons was full of cavities. It seems that the cavities on the surface of the carbons resulted from the removal of active agents leaving empty space previously occupied by the active agent. Consequently, the reaction with KOH was aiding in the creation of the porous structure and was proved to be an effective activating agent for the production of high-surface area CWZ-22. Moreover, **Figure 3b–d** shows irregular surface of ACs, the grooves that are considered helpful for the accessibility of gases to the adsorbent surface.
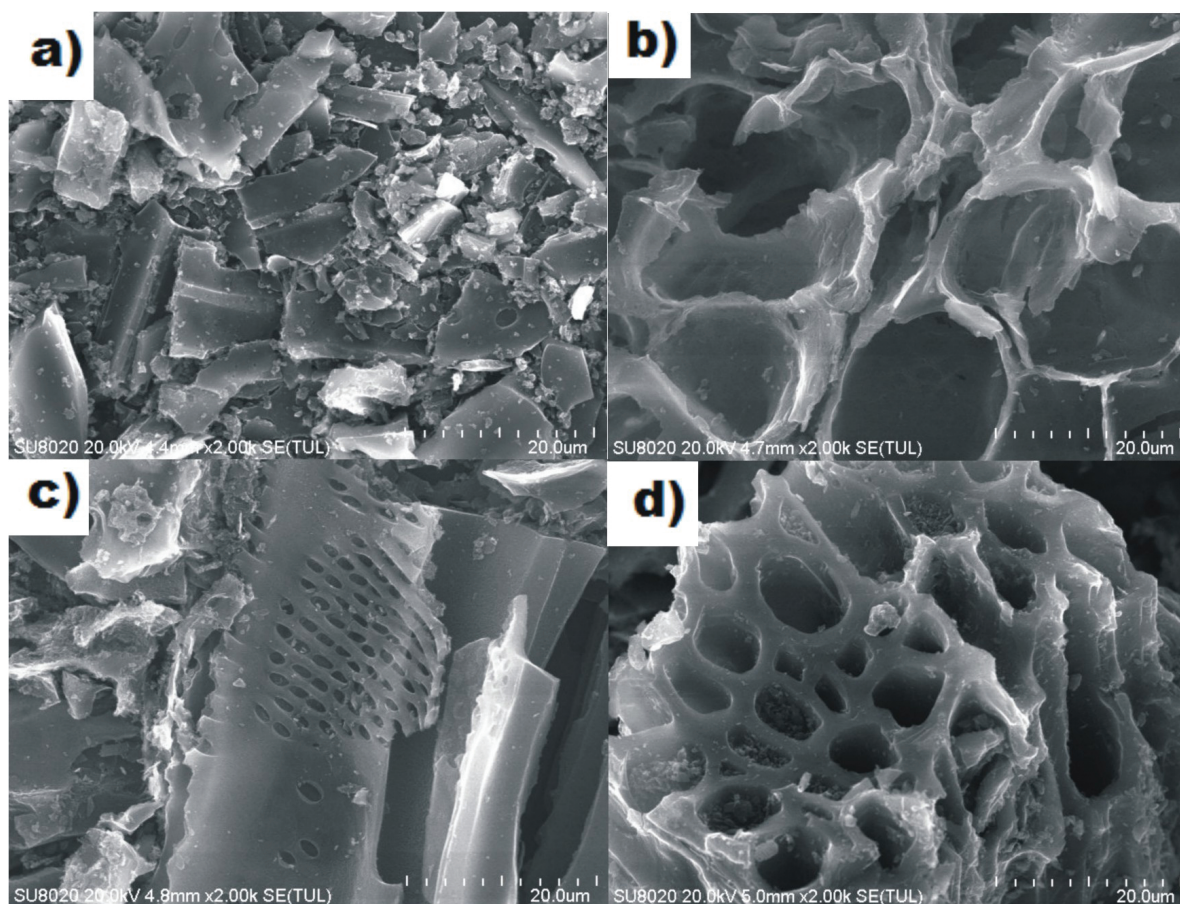

Figure 3. SEM images of the (a) pristine CWZ-22 (b) KOH:CWZ-22 = 1, (c) KOH:CWZ-22 = 2, and (d) KOH:CWZ-22 = 4.

3.3. X-ray diffraction studies

The XRD patterns of pristine CWZ-22 and of the samples with mass ratio from KOH:CWZ-22 = 1 to KOH:CWZ-22 = 4 are shown in **Figure 4**.
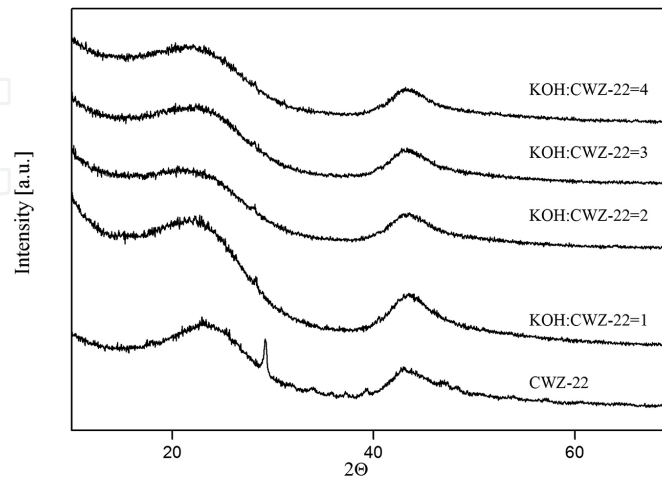

Figure 4. XRD patterns of the ACs.

According to the XRD patterns, the position of peaks is similar for all carbon samples. There are only two peaks at about 23 and 43 2θ in the XRD pattern corresponding to the (002) and (101) planes of the hexagonal graphite (JCPDS, 75-1621). The peaks are very broad because of the random turbostratic stacking of a limited number of layers.

3.4. FTIR analysis

To characterize surface groups on activated carbon, FTIR (Fourier transform infrared) transmission spectra were obtained. The spectra of starting commercial CWZ-22 and modified CWZ-22 were presented in **Figure 5**.
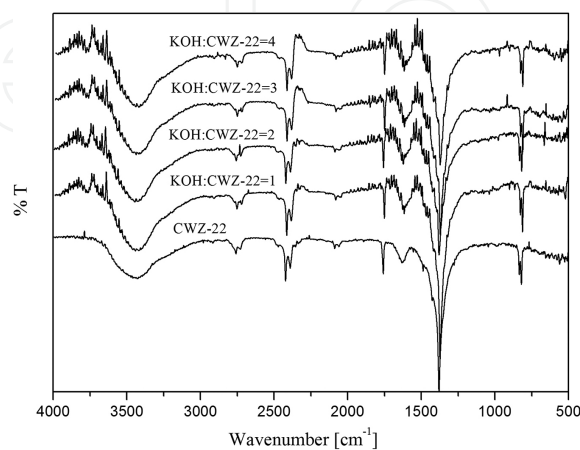

Figure 5. FTIR spectra of activated carbons CWZ-22.

The FTIR spectroscopy provides information on the chemical structure of materials. It can be observed in the **Figure 6** that irrespectively of a KOH/AC ratio, the overall shape of the spectra is very similar. The band at around 3440 cm^{-1} is assigned to the O–H stretching of physisorbed water [27, 28] and that at 1650 cm^{-1}—to a presence of physisorbed water as well as of chemisorbed CO_2. All the spectra show a band in the region 2360–2344 cm^{-1} due to CO_2 in air [28]. The broader peaks about 1760 cm^{-1} are characteristic for C=O stretching vibration in carboxylic groups. The peaks around 1380 cm^{-1} can be assigned to the deformation vibrations of an H–C–OH group [29]. The bands located around 2750 and 820 cm^{-1} could be assigned to C–H group.
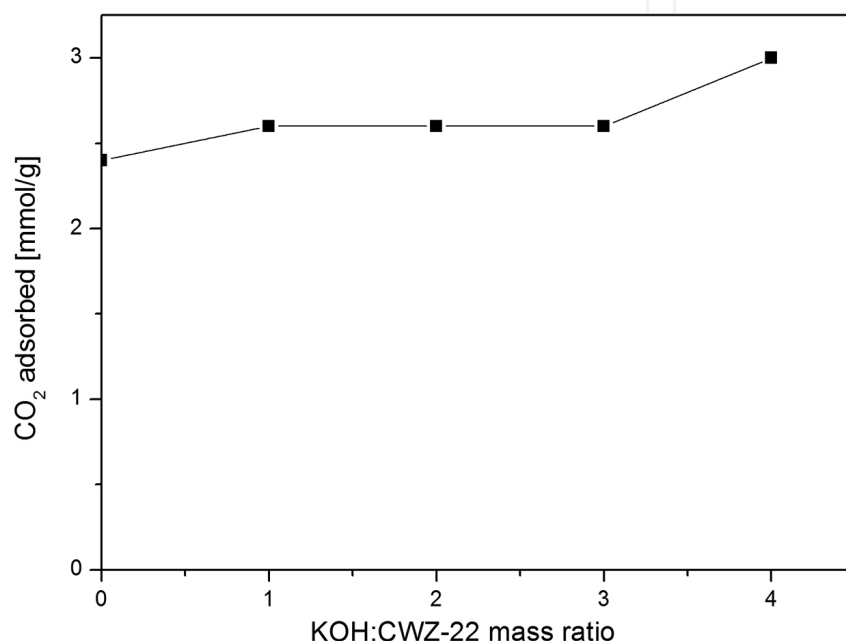

Figure 6. Influence of KOH:CWZ-22 mass ratio on the adsorbed of CO_2 at 1 bar at temperature 25°C.

The FTIR spectra of ACs modified KOH do not exhibit any differences compared to carbon CWZ-22, and these ACs present similar characteristics in their study by the FTIR technique. This suggests that the adsorption capacity of activated carbons CWZ-22 is not depending on the chemical reactivity of functional groups at surface.

3.5. Effect of KOH:CWZ-22 mass ratio of activated carbon on CO_2 adsorption

Preliminary research on CO_2 adsorption was performed at the temperature of 25°C and pressure up to of 1 bar. Chemical activation by KOH increased CO_2 adsorption compared to pristine sample. The difference was small for KOH:CWZ-22 mass ratio 1–3, but when KOH:CWZ-22 was equal to 4, the CO_2 adsorption was considerably higher.

3.6. CO_2 adsorption and modeling of adsorption data

Two ACs samples were chosen for the modeling of adsorption data—the pristine sample and AC with the highest CO_2 adsorption at the temperature of 25°C, namely KOH:CWZ-22 = 4.

The adsorption isotherms were measured at temperatures 25, 40, 60, 80, and 100°C up to the pressure equal to 2 bar. Adsorption isotherms of CO_2 adsorbed on CWZ-22 and KOH:CWZ-22 = 4 at different temperatures are presented in **Figures 7** and **8**, respectively.

Figure 7. CO_2 adsorption on CWZ-22 in different temperatures. Symbols denote experimental data, and lines correspond to the predictions from the (a) Langmuir, (b) Freundlich, (c) Sips, and (d) Toth isotherm models.
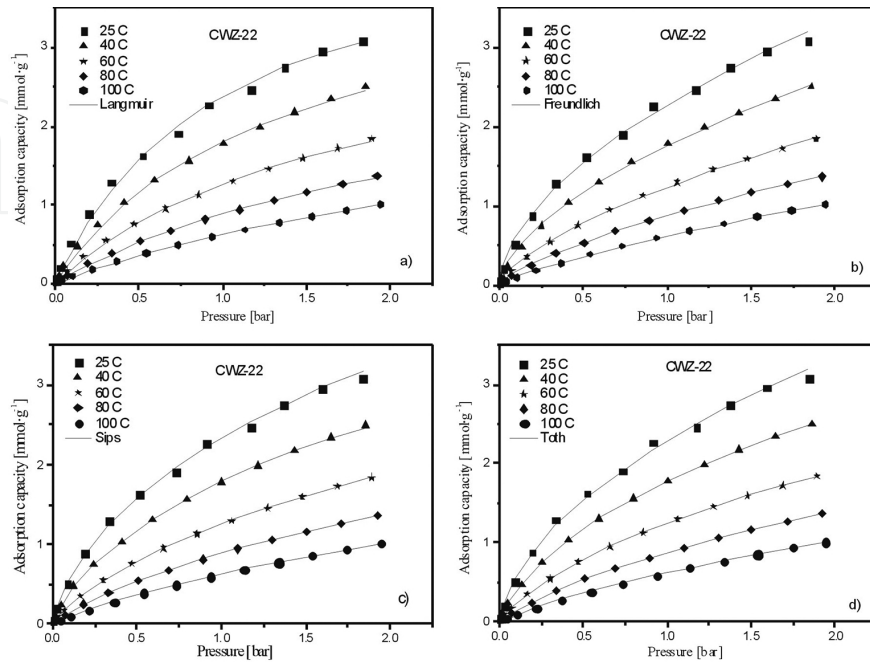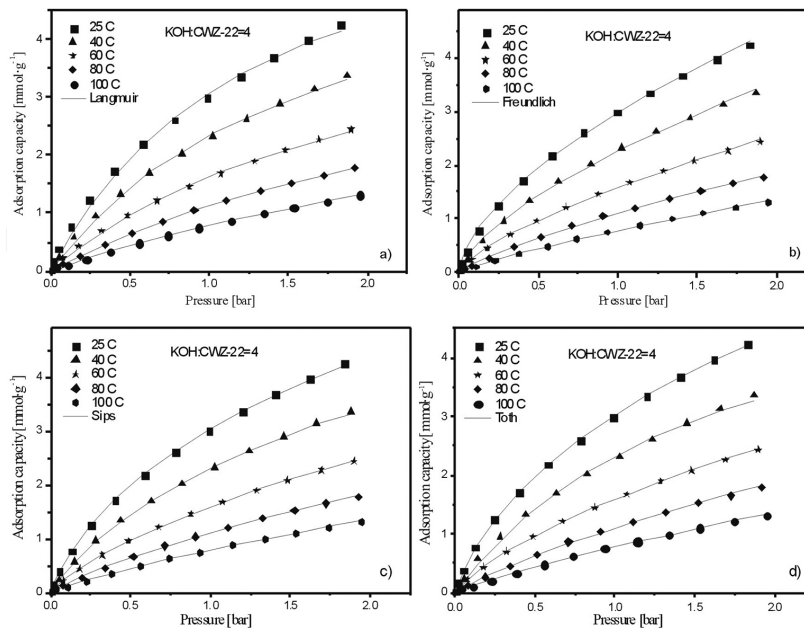

Figure 8. CO_2 adsorption on KOH:CWZ-22 = 4 at different temperatures. Symbols denote experimental data, and lines are predictions from the (a) Langmuir, (b) Freundlich, (c) Sips, and (d) Toth isotherm models.

As it is clearly seen in the **Figures 7** and **8**, the amount of CO$_2$ uptake increases with an increase in pressure and decreases with increasing adsorption temperature.

The amount of CO$_2$ adsorbed on the KOH:CWZ-22 = 4 was higher than on the pristine carbon at all temperatures. The adsorption of CO$_2$ on KOH:CWZ-22 = 4 at 2 bar and 25°C was of 38% higher than on the CWZ-22.

The Langmuir, Freundlich, Toth, and Sips models were employed to describe the adsorption data of CO$_2$ onto the nonmodified and modified CWZ-22. The fitted adsorption isotherms are presented in **Figures 7** and **8**. Lines show the Langmuir, Freundlich, Toth, and Sips isotherm used to describe adsorption values. The experimental data were marked as symbols. The parameters of model isotherms of Langmuir, Freundlich, Toth, and Sips obtained from a nonlinear fit to experimental data at multiple temperatures for each adsorbate are shown in **Tables 2** and **3**.

Adsorbent	T [°C]	Langmuir			Freundlich		
		q_m [mmol•g^{-1}]	b_L	R^2	k_F [mmol•g^{-1}]	n_F	R^2
CWZ-22	25	4.50	1.13	0.999	2.28	0.55	0.999
	40	4.01	0.84	0.999	1.75	0.60	0.999
	60	3.40	0.60	0.999	1.23	0.66	0.999
	80	2.94	0.44	0.999	0.87	0.71	0.999
	100	2.61	0.32	0.999	0.62	0.76	0.999
KOH:CWZ-22 = 4	25	6.98	0.80	0.999	2.97	0.62	0.999
	40	6.26	0.60	0.999	2.25	0.67	0.999
	60	5.13	0.46	0.999	1.57	0.70	0.999
	80	4.78	0.31	0.999	1.09	0.77	0.999
	100	4.27	0.23	0.999	0.77	0.82	0.999

Table 2. Parameters of Langmuir and Freundlich models for CO$_2$ adsorption onto the CWZ-22 and KOH:CWZ-22 = 1.

A good agreement can be noticed between the experimental data and the model fitting. This indicates that these models can accurately explain the correlation of the adsorption equilibrium with the adsorbent. According to the R^2 parameter, all the fitted data for the four models are good. In all of the cases, the obtained regression coefficient R^2 is higher than 0.999. Thus, in order to analyze the impact of various error functions on the predicted isotherms, four different error functions namely SSE, HYBRID, MPSD, and ARE were used by nonlinear regression method to recognize the error distribution between the experimental equilibrium data and the isotherms studied. Their values are presented in **Table 4**. The best fit isotherm was selected based on the error function. The lowest values of the error functions are bolded.

Adsorbent	T [°C]	Toth				Sips			
		q_m [mmol•g^{-1}]	b_T	n_T	R^2	q_m [mmol•g^{-1}]	b_S	n_S	R^2
CWZ-22	25	49.71	0.89	0.36	0.999	7.60	0.44	0.74	0.999
	40	28.56	0.13	0.17	0.999	7.78	0.30	0.75	0.999
	60	16.95	0.18	0.32	0.999	6.24	0.25	0.80	0.999
	80	18.74	0.10	0.35	0.999	5.29	0.20	0.84	0.999
	100	14.85	0.08	0.44	0.999	4.41	0.17	0.88	0.999
KOH:CWZ-22 = 4	25	49.60	0.13	0.19	0.999	13.52	0.44	0.76	0.999
	40	43.57	0.28	0.44	0.999	9.83	0.31	0.84	0.999
	60	22.45	0.11	0.35	0.999	9.80	0.26	0.83	0.999
	80	6.60	0.24	0.81	0.999	5.33	0.26	0.97	0.999
	100	6.24	0.16	0.81	0.999	4.95	0.19	0.97	0.999

Table 3. Parameters of Toth and Sips models for CO_2 adsorption onto the CWZ-22 and KOH:CWZ-22 = 1.

	T [°C]	SSE	HYBRID	ARE	MPSD
Langmuir					
CWZ-22	25	0.0621	0.9452	12.2430	24.7905
	40	0.0277	0.5980	8.8268	17.3420
	60	0.0084	0.2504	6.4789	12.7745
	80	0.0024	0.1060	5.9659	12.7569
	100	0.0007	0.0429	3.7235	7.5719
KOH:CWZ-22 = 4	25	0.0730	0.8836	8.3028	15.9486
	40	0.0219	0.2412	4.9931	8.5596
	60	0.0100	0.2578	5.8876	12.0723
	80	0.0005	0.0343	3.0568	8.9733
	100	0.0006	0.0721	3.5310	10.9968
Freundlich					
CWZ-22	25	0.0488	0.9486	12.6447	28.6932
	40	0.0122	0.4071	7.3336	17.5881
	60	0.0054	0.2116	5.9238	13.3919
	80	0.0020	0.1301	6.9945	17.4743
	100	0.0009	0.0575	4.2344	8.9907
KOH:CWZ-22 = 4	25	0.0340	0.7104	7.4561	18.0023
	40	0.0291	1.9369	18.4177	55.9929

	T [°C]	SSE	HYBRID	ARE	MPSD
	60	0.0062	0.1653	4.7272	10.1948
	80	0.0066	0.2695	7.7422	16.0321
	100	0.0025	0.1165	4.5893	9.9664
Sips					
CWZ-22	25	**0.0158**	**0.0827**	**2.0922**	**3.0187**
	40	**0.0003**	**0.0132**	**1.2073**	**3.4548**
	60	**0.0001**	0.0022	**0.2922**	0.9428
	80	**0.0001**	**0.0009**	0.7967	**1.1036**
	100	**0.0002**	**0.0010**	**0.3740**	**0.9455**
KOH:CWZ-22 = 4	25	**0.0014**	**0.0360**	**1.5490**	**4.2991**
	40	0.0028	**0.1062**	**5.7191**	**8.1221**
	60	**0.0001**	0.0009	0.2904	0.5330
	80	**0.0003**	**0.0309**	**2.8569**	**7.7200**
	100	**0.0005**	**0.0678**	**3.5893**	**9.3992**
Toth					
CWZ-22	25	0.0159	0.1261	3.9734	9.8499
	40	0.0022	0.0708	2.9383	7.0922
	60	0.0003	**0.0011**	0.3645	**0.7170**
	80	0.0004	0.0012	**0.6290**	1.6090
	100	0.0003	0.0012	0.5325	1.5068
KOH:CWZ-22 = 4	25	0.0046	0.1036	2.7307	6.7459
	40	**0.0020**	0.2330	5.8074	20.7130
	60	0.0001	0.0040	0.6231	1.8645
	80	0.0004	0.0339	2.9728	8.4997
	100	0.0007	0.0733	3.6244	10.9437

Table 4. The error values of isotherm models for adsorption of CO_2 by CWZ-22 and KOH:CWZ-22 = 4.

The Sips model results in a much better fitting for CO_2 adsorption than Langmuir, Freundlich, and Toth models under the entire experimental temperature range.

Table 3 lists the optimal isotherm parameters obtained by simultaneously fitting of all the adsorption equilibrium data at multiple temperatures for carbons CWZ-22 and KOH:CWZ-22 = 4. The excellent agreement between the model fittings and the experimental data demonstrates that these isotherm models can be confidently employed to accurately correlate the adsorption equilibria of the adsorbates. As it is observed, decreasing the temperature increases the maximum of the adsorbed amount (q_m) in all isotherms. In other words, increasing

temperature will decrease the amount adsorbed at a given pressure. The parameter b_s is the adsorption affinity, whereas n_s qualitatively characterizes the heterogeneity of the adsorbate adsorbent system. Also, it can be seen that affinity parameter (b_s) increases with a decrease in temperature. In fact, at lower temperatures, the surface is covered more by the molecules which lead to the stronger affinity of adsorbate molecules towards the surface. The b_s parameters calculated for unmodified and modified carbons are very similar so affinity of CO_2 molecules towards the surface of this two ACs is similar. The surfaces of both ACs were homogenous because n_s was higher than 0.5. The values of n_s for KOH:CWZ-22 = 4 were higher than for the CWZ-22. The modification makes the surface more homogenous. The fitting parameters (qm, b_s, and n_s) of Sips isotherm equations are temperature dependent and defined as Eqs. (6)–(8) [30].

$$q_m = q_{m0} \exp\left[\chi\left(1 - \frac{T_0}{T}\right) \right] \tag{6}$$

$$b_s = b_{s0} \exp\left[\frac{Q}{RT_0}\left(\frac{T_0}{T} - 1\right) \right] \tag{7}$$

$$n_s = n_{s0} + \alpha\left(1 - \frac{T_0}{T}\right) \tag{8}$$

The parameters q_{m0}, b_{s0}, n_{s0} are the parameters q_m, b_s, n_s, respectively, at the same reference temperature (T_0) The χ and α are constant parameters. In Langmuir equation, Q is equal to isosteric heat of adsorption, constant with surface coverage. The parameter Q in the Sips equation is only the measure of the adsorption heat. The parameter Q defined in the affinity constant b_s is the isosteric heat at the fractional loading of 0.5.

	α	Q [kJ/mol]	χ
CWZ-22	0.70	12.08	−2.25
KOH:CWZ-22 = 4	1.10	6.66	−4.91

Table 5. Parameters of Eqs. (6)–(8).

The temperature-dependent equations of the exponent n_s and saturation capacity q_m are empirical, and such forms in Eqs. (6) and (8) were chosen arbitrary because of their simplicity. Because Eqs. (6) and (8) have not been derived from physical laws, then, as a result, the parameters χ and α have no physical meaning.

The unknown parameters of Eqs. (6)–(8) were determined using Excel's Solver to minimize the sum of squared error. The correlated parameters are listed in **Table 5**.

The plots of observed versus predicted values of parameters q_{ms}, b_s, and n_s showed good agreement between these values (**Figure 9**).
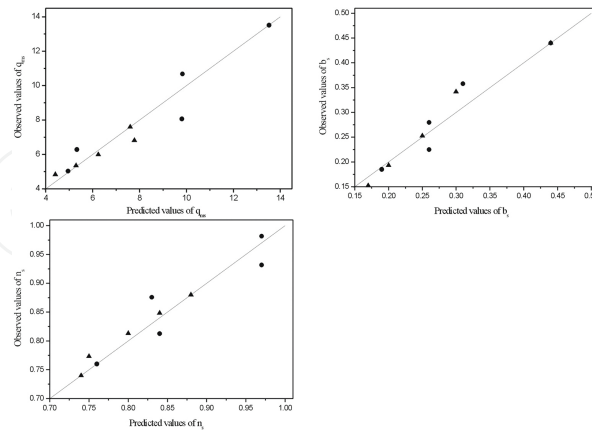

Figure 9. Plot of the observed versus predicted values parameters q_{ms}, b_s, and n_s for CWZ-22 (▲), KOH:CWZ-22 = 4 (●).

On the basis of Eqs. (3), (6)–(8) and values from **Table 3**, A, the adsorption capacity on CWZ-22 and KOH:CWZ-22 = 4 at any temperature can be calculated.

3.7. Isosteric heat of adsorption

The heat of adsorption is described as an indicator of the interaction strength between the adsorbate molecules and the adsorbent. Isosteric heat of adsorption as a function of surface coverage (defined as number of adsorbed molecules on a surface divided by the number of molecules in a filled monolayer on that surface) at different temperatures was calculated by applying the Clausius–Clapeyron equation. The Sips isotherm model was used here for an evaluation of isosteric heat of adsorption. The Q_i of CWZ-22 and KOH:CWZ-22 = 4 was determined from the slope of the straight line after plotting $\ln(p)$ against $1/T$ for different surface coverage (θ), as shown in **Figure 10**.

The isosteric heat of adsorption for CWZ-22 and KOH:CWZ-22 = 4 is shown as a function of surface coverage in **Figure 11**. The isosteric heats of adsorption decreased with the surface
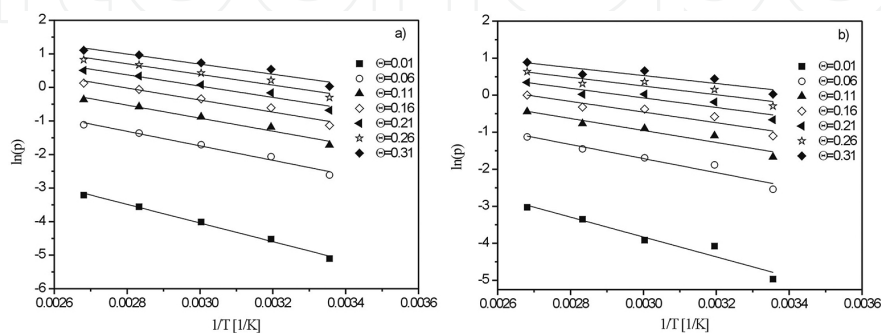

Figure 10. Adsorption isostere for determining isosteric heat of adsorption for ACs: (a) CWZ-22, (b) KOH:CWZ-22 = 4.

coverage increase. For the both ACs at the "zero loading," isosteric heats of adsorption tend to 30 kJ/mol. This value indicates the physisorption. The modification of CWZ-22 reduced the isosteric heat of adsorption. By extrapolation, the curves to surface coverage equal to 0.5 were found that the isosteric heat of adsorption for CWZ and KOH:CWZ-22 = 4 was equal to 10 and 6 kJ/mol, respectively. These values are similar to values obtained on the basis of Eq. (7) and presented in **Table 5**.
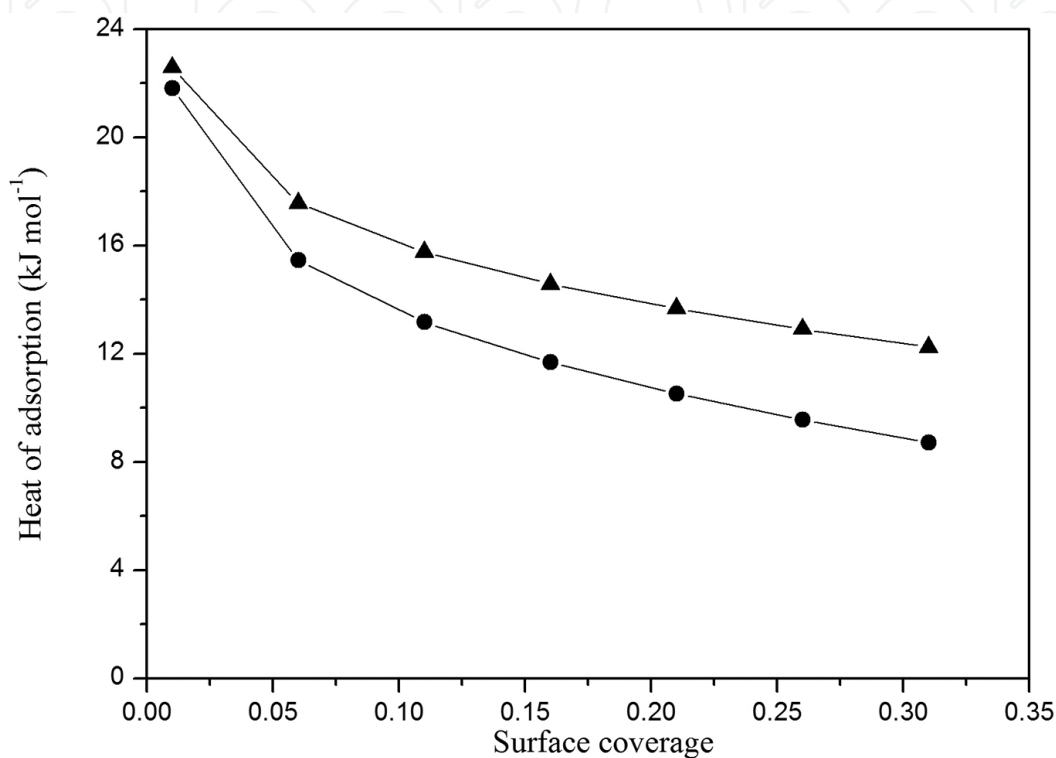

Figure 11. Isosteric heat of adsorption for CO_2 on (▲) CWZ-22 and (−) KOH:CWZ-22 = 4.

4. Conclusions

The impregnation of CWZ-22 by KOH highly effectively increased the porosity, specific surface area, and pore volume of ACs. The specific surface area of KOH:CWZ-22 = 4 significantly increased to 1299 m^2/g as compared with pristine CWZ-22 (856 m^2/g). Similarly, the total pore volume raised from 0.51 to 0.77 cm^3/g.

The chemical modification of CWZ-22 increased the CO_2 adsorption capacity of 38%. The CO_2 adsorption capacity of 4.24 mmol/g obtained for the KOH:CWZ-22 = 4 was considerably higher than that for pristine CWZ-22 (3.08 mmol/g) at 25°C and 2 bar. The Sips model described very good the CO_2 adsorption on KOH:CWZ-22 = 4 and in the pristine sample. The surface of the both ACs was homogenous. The values of isosteric heats of adsorption indicated on physisorption.

Acknowledgements

Author details

Joanna Sreńscek-Nazzal, Urszula Narkiewicz, Antoni W. Morawski, Rafał J. Wróbel and Beata Michalkiewicz*

*Address all correspondence to: Beata.Michalkiewicz@zut.edu.pl

Institute of Inorganic Technology and Environment Engineering, The West Pomeranian University of Technology in Szczecin, Szczecin, Poland

References

[1] Chen T, Deng S, Wang B, Huang J, Wang Y, Yu G. CO$_2$ adsorption on crab shell derived activated carbons: contribution of micropores and nitrogen containing groups. RSC Advances. 2015;5:48323–48330. doi:10.1039/C5RA04937G

[2] Deng S, Wei H, Chen T, Wang B, Huang J, Yu G. Superior CO$_2$ adsorption on pine nut shell-derived activated carbons and the effective micropores at different temperatures. Chemical Engineering Journal. 2014;253:46–54. doi:10.1016/j.cej.2014.04.115

[3] Li P, Tezel FH. Adsorption separation of N$_2$, O$_2$, CO$_2$ and CH$_4$ gases by beta-zeolite. Microporous and Mesoporous Materials. 2007;98:94–101. doi:10.1016/j.micromeso. 2006.08.016

[4] Wu D, Xu Q, Liu D, Zhong C. Exceptional CO$_2$ capture capability and molecular-level segregation in a Li-modified metal-organic framework. Journal of Physical Chemistry C. 2010;114:16611–16617. doi:10.1021/jp105899t

[5] Linneen N, Pfeffer R, Lin YS. CO$_2$ capture using particulate silica aerogel immobilized with tetraethylenepentamine. Microporous and Mesoporous Materials. 2013;176:123–131. doi:10.1016/j.micromeso.2013.02.052

[6] Sreńscek-Nazzal J, Narkiewicz U, Morawski AW, Wróbel R, Michalkiewicz B. Comparison of optimized isotherm models and error functions for carbon dioxide adsorption on activated carbon. Journal of Chemical & Engineering Data. 2015;60:3148–3158. doi:10.1021/acs.jced.5b00294

[7] Sreńscek Nazzal J, Glonek K, Młodzik J, Narkiewicz U, Morawski AW, Wróbel R, Michalkiewicz B. Increase the microporosity and CO_2 adsorption of a commercial activated carbon. Applied Mechanics and Materials. 2015;749:17–21. doi:10.4028/www.scientific.net/AMM.749.17

[8] Deng S, Hu B, Chen T, Wang B, Huang J, Wang Y, Yu G. Activated carbons prepared from peanut shell and sunflower seed shell for high CO_2 adsorption. Adsorption. 2015;21:125–133. doi:10.1007/s10450-015-9655-y

[9] Lee SY, Yoo HM, Park SW, Park SH, Oh YS, Rhee KY, Park SJ. Preparation and characterization of pitch-based nanoporous carbons for improving CO_2 capture. Journal of Solid State Chemistry. 2014;215:201–205. doi:10.1016/j.ssc.2014.03.038

[10] Ello AS, Souza LKC, Trokourey A, Jaroniec M. Development of microporous carbons for CO_2 capture by KOH activation of African palm shells. Journal of CO_2 Utilization. 2013;2:35–38. doi:10.1016/j.jcou.2013.07.003

[11] Hu Z, Srinivasan MP. Preparation of high-surface-area activated carbons from coconut shell. Microporous and Mesoporous Materials. 1999;27:11–18. doi:10.1016/s1387-1811(98)00183-8

[12] Olivares-Marín M, Maroto-Valer MM. Preparation of a highly microporous carbon from a carpet material and its application as CO_2 sorbent. Fuel Processing Technology. 2011;92:322–329. doi:10.1016/j.fuproc.2010.09.022

[13] Sevilla M, Fuertes AB. Sustainable porous carbons with a superior performance for CO_2 capture. Energy & Environmental Science. 2011;4:1765–1771. doi:10.1039/C0EE00784F

[14] Shen W, He Y, Zhang S, Li J, Fan W. Yeast-based microporous carbon materials for carbon dioxide capture. ChemSusChem. 2012;5:1274–1279. doi:10.1002/cssc.201100735

[15] Glonek K, Sreńscek-Nazzal J, Narkiewicz U, Morawski AW, Wróbel RJ, Michalkiewicz B. Preparation of activated carbon from beet molasses and TiO_2 as the adsorption of CO_2. Acta Physica Polonica A. 2016;129:158–161. doi:10.12693/APhysPolA.129.158

[16] Mourao PAM, Laginhas C, Custódio F, Nabais JMV, Carrott PJM, Ribeiro Carrott MML. Influence of oxidation process on the adsorption capacity of activated carbons from lignocellulosic precursors. Fuel Processing Technology. 2011;92:241–246. doi:10.1016/j.fuproc.2010.04.013

[17] Heidari A, Younesi H, Rashidi A, Ghoreyshi AA. Adsorptive removal of CO_2 on highly microporous activated carbons prepared from Eucalyptus camaldulensis wood: effect of chemical activation. Journal of the Taiwan Institute of Chemical Engineers. 2014;45:579–588. doi:10.1016/j.jtice.2013.06.007

[18] Ning P, Li F, Yi H, Tang X, Peng J, Li Y, He D, Deng H. Adsorption equilibrium of methane and carbon dioxide on microwave-activated carbon. Separation and Purification Technology. 2012;98:321–326. doi:10.1016/j.seppur.2012.07.001

[19] Hameed BH, Mahmoud DK, Ahmad AL. Equilibrium modeling and kinetic studies on the adsorption of basic dye by a low-cost adsorbent: coconut (*Cocos nucifera*) bunch waste. Journal of Hazardous Materials. 2008;158:65–72. doi:10.1016/j.jhazmat. 2008.01.034

[20] Foo KY, Hameed BH. Insights into the modeling of adsorption isotherm systems. Chemical Engineering Journal. 2010;156:2–10. doi:10.1016/j.cej.2009.09.013

[21] Salmasi M, Fatemi S, Doroudian-Rad M, Jadidi F. Study of carbon dioxide and methane equilibrium adsorption on silicoaluminophosphate-34 zeotype and T-type zeolite as adsorbent. International Journal of Environmental Science and Technology. 2013;10:1067–1074. doi:10.1007/s13762-013-0334-9

[22] Ma J, Si C, Li Y, Li R. CO$_2$ adsorption on zeolite X/activated carbon composites. Adsorption. 2012;18:503–510. doi:10.1007/s10450-012-9440-0

[23] Behvandi A, Tourani S. Equilibrium modeling of carbon dioxide adsorption on zeolites. Chemical and Molecular Engineering. 2011;5:351–353. doi:scholar.waset.org/ 1999.2/6186

[24] Kumar KV, Porkodi K, Rocha F. Comparison of various error functions in predicting the optimum isotherm by linear and non-linear regression analysis for the sorption of basic red 9 by activated carbon. Journal of Hazardous Materials. 2008;150:158–165. doi: 10.1016/j.hazmat.2007.09.020

[25] Porter JF, McKay G, Choy KH. The prediction of sorption from a binary mixture of acidic dyes using single- and mixed-isotherm variants of the ideal adsorbed solute theory. Chemical Engineering Science. 1999;54:5863–5885. doi:10.1016/ s0009-2509(99)00178-5

[26] Marquardt DW. An algorithm for least-squares estimation of nonlinear parameters. Journal of the Society for Industrial and Applied Mathematics. 1963;11:431–441.

[27] Yang K, Peng J, Srinivasakannan C, Xia D, Duan X. Preparation of high surface area activated carbon from coconut shells using microwave heating. Bioresource Technology. 2010;101:6163–6169. doi:10.1016/j.biortech.2010.03.001

[28] Murugan C, Bajaj HC, Jasra RV. Transesterification of propylene carbonate by methanol using KF/Al$_2$O$_3$ as an efficient base catalyst. Catalysis Letters. 2010;137:224–231. doi: 10.1007/s10562-010-0348-6

[29] Li Y, Zijll M, Chiang S, Pan N. KOH modified graphene nanosheets for supercapacitor electrodes. Journal of Power Sources. 2011;196:6003–6006. doi:10.1016/j.jpowsour. 2011.02.092

[30] Do DD. Adsorption analysis: equilibria and kinetics. Imperial College Press, London. 1998;57–64.